Fuel 153 (2015) 361–369

Contents lists available at ScienceDirect

Fuel

journal homepage: www.elsevier.com/locate/fuel

Promotional effect of CeO_2 modified support on V_2O_5–WO_3/TiO_2 catalyst for elemental mercury oxidation in simulated coal-fired flue gas

Lingkui Zhao, Caiting Li *, Jie Zhang, Xunan Zhang, Fuman Zhan, Jinfeng Ma, Yin'e Xie, Guangming Zeng

College of Environmental Science and Engineering, Hunan University, Changsha 410082, PR China
Key Laboratory of Environmental Biology and Pollution Control (Hunan University), Ministry of Education, Changsha 410082, PR China

HIGHLIGHTS

- Nano-sized TiO_2–CeO_2 mixed oxides is used as support material for Hg^0 oxidation.
- The Hg^0 oxidation activity of VWTi was promoted by support modification.
- There was synergistic effect between V_2O_5 and CeO_2 on Hg^0 oxidation.
- Hg^0 oxidation over $V_{0.80}WTiCe_{0.25}$ follows a Mars–Maessen mechanism.

GRAPHICAL ABSTRACT

Mechanism of CeO_2 modified V_2O_5–WO_3/TiO_2 catalysts for elemental mercury oxidation.

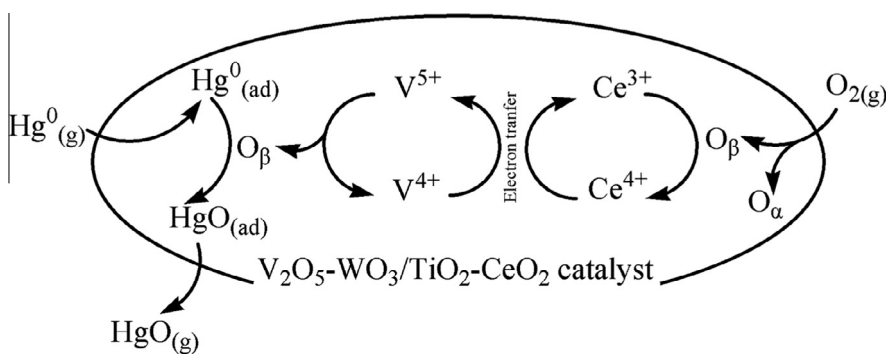

ARTICLE INFO

Article history:
Received 8 October 2014
Received in revised form 21 January 2015
Accepted 2 March 2015
Available online 20 March 2015

Keywords:
V_2O_5–WO_3/TiO_2
Catalytic oxidation
Elemental mercury
Flue gas
CeO_2

ABSTRACT

In order to enhance the catalytic activity for elemental mercury (Hg^0) oxidation without the aid of HCl, CeO_2 was added into the support to modify V_2O_5–WO_3/TiO_2 catalysts. The performance of V_2O_5–WO_3/TiO_2–CeO_2 (VWTiCe) catalysts on Hg^0 oxidation as well as the catalytic mechanism was also studied. The catalysts were characterized by BET, XRD and XPS techniques. The results showed that the performance on Hg^0 oxidation was promoted by the introduction of CeO_2. NO and SO_2 has a promoting effect on Hg^0 oxidation in the presence of O_2. Besides, the inhibitive effect of NH_3 on Hg^0 oxidation was confirmed by NH_3 consuming the surface oxygen of catalyst. The addition of CeO_2 improved the ability to resist H_2O. Results also indicated that the Hg^0 oxidation efficiencies of $V_{0.80}WTiCe_{0.25}$ catalysts were thought to be aided by synergistic effect between V_2O_5 and CeO_2. Hg^0 oxidation over $V_{0.80}WTiCe_{0.25}$ follows a Mars–Maessen mechanism where lattice oxygen of V_2O_5 reacts with adjacently absorbed Hg^0.

1. Introduction

Mercury pollution has received considerable attention from environmental researchers due to its high volatility, long persistence, and strong bioaccumulative properties [1–3]. Coal combustion is a significant fraction of anthropogenic source of mercury emission [4]. In January 2013, 140 nations adopted the first legally binding international treaty to set enforceable limits on emissions of mercury and exclude, phase out, or restrict some products that contain mercury [5].

A number of technologies have been used for mercury control from coal combustion flue gas, such as sorbent injection [6], catalytic oxidation [7] and photochemical oxidation [8]. It was reported [9] that the efficiency of mercury control methods

* Corresponding author at: College of Environmental Science and Engineering, Hunan University, Changsha 410082, PR China. Tel./fax: +86 731 88649216.
E-mail addresses: ctli@hnu.edu.cn, ctli3@yahoo.com (C. Li).

http://dx.doi.org/10.1016/j.fuel.2015.03.001
0016-2361/

depends largely on the form of mercury. Mercury in the flue gas from coal combustion is often classified into three forms, i.e. elemental mercury (Hg^0), oxidized mercury (Hg^{2+}), and particle-associated mercury (Hg^P) [10–12]. Hg^{2+} and Hg^P can be easily removed by existing air pollution control installations such as fabric filters (FF), cold-side or hot-side electrostatic precipitators (ESPs), wet or dry flue gas desulfurization (FGD) and selective catalytic reduction (SCR) [13]. However, Hg^0 is much difficult to be capture by air pollution control devices because of its high volatility and nearly insolubility in water [14–16]. Therefore, development of viable technologies for the effective conversion of Hg^0 to Hg^{2+} has become the focus of many investigations in recent years. With extensive application of the SCR technology in coal-fired power plants, lots of full-scale tests have been carried out to evaluate the performance of the SCR catalysts on Hg^0 oxidation [16–19]. As a typical commercial NH_3–SCR catalyst, V_2O_5–WO_3/TiO_2 catalysts not only show high catalytic activity for NO reduction but also exhibit the co-benefit of promoting mercury oxidation [20]. Consequently, a low cost option for control of mercury from coal fired power plants can be achieved by this co-benefit of SCR installation.

It is well-known that the involved oxidants are mainly oxygen and chlorine in real flue gas. However, in China, the chlorine content of feed-coal (63–318 mg/kg) is much lower than that of US coals (628 mg/kg) [21–23]. Thus, catalytic oxidation of Hg^0 using gaseous oxygen as the oxidant is an environment-friendly and economical method for Hg^0 control. However, the conventional SCR catalysts were not effective enough for Hg^0 oxidation in the absence of HCl. Accordingly, how to improve the catalytic activity for Hg^0 oxidation without HCl has become an important research scope the co-benefit performance of SCR catalysts. Up to now, many kinds of catalysts have been investigated for SCR such as metal oxides supported on TiO_2 [24–26]. However, TiO_2 still exhibits some drawbacks where improvements can be made, such as low surface area [27,28]. In general, appropriate active sites, high-surface-area supports, and their interaction are important to the activity of the catalysts [29]. Thus, in order to improve the properties of TiO_2, the sol–gel method was used to synthesize nano-sized CeO_2–TiO_2 carriers. It has been reported that TiO_2–CeO_2 mixed oxide is a promising catalyst for the SCR of NO with NH_3 in the presence of oxygen [30,31]. A Ce–Ti based (CeO_2–TiO_2) catalyst showed excellent NH_3–SCR activity, high N_2 selectivity, broad operation temperature window, and high resistance to space velocity [32]. What is more, for CeTi catalyst, the combination of SO_2 and NO without HCl resulted in high Hg^0 oxidation efficiency [33]. Accordingly, CeO_2–TiO_2 mixed oxide is extensively studied for emission control. It is well known that cerium has two stable oxidation states (Ce^{3+} and Ce^{4+}), which could provide cerium with significant oxygen storage capability through the redox shift between the two oxidation states [34]. Meanwhile, CeO_2 has been studied for Hg^0 oxidation and it could enhance catalytic activity due to its oxygen storage capability by storing or releasing O via the Ce^{4+}/Ce^{3+} redox couple [35]. Furthermore, CeO_2 based catalysts were reported to have resistance to the effect of water vapor [30,33]. Consequently, CeO_2 is widely used in composite materials and as a catalyst support material [36]. However, catalysts with nano-sized TiO_2–CeO_2 composite oxides carrier such as V_2O_5–WO_3/TiO_2–CeO_2 for Hg^0 oxidation without HCl and the catalytic mechanism have rarely been reported.

The present work aimed to improve mercury oxidation activity without the aid of HCl as well as reveal the catalytic mechanism of CeO_2 modified support on V_2O_5–WO_3/TiO_2 catalysts. A series of experiments and characterizations were carried out to probe into the superiority of catalyst with nano-sized TiO_2–CeO_2 composite oxide carriers. Besides, the effects of individual flue gas components on Hg^0 oxidation were also studied.

2. Experimental section

2.1. Reagents

All the reagents used in this work were analytical pure grade (AR), including: The anatase-type nanosize TiO_2 powder (99.8%, Chengdu Ai Keda Chemical Technology Co.), cerium nitrate (99.0%, Kemiou Chemical Reagent Co.), anhydrous ethanol (99.7%, Kemiou Chemical Reagent Co.), nitric acid (68.0%, Sinopharm Chemical Reagent Co), butyl titanate (99.0%, Kemiou Chemical Reagent Co.), ammonium wolframate (90.0%, Sinopharm Chemical Reagent Co), ammonium metavanadate (99.0%, Kemiou Chemical Reagent Co.) and Oxalic acid (99.5%, Sinopharm Chemical Reagent Co). Ultrapure water was applied to prepare the required solutions.

2.2. Preparation of catalysts

TiO_2–CeO_2 composite oxide carriers were prepared by a sol–gel method. Specifically as follows: a certain amount of cerium nitrate, anhydrous ethanol (0.6 mol), ultrapure water (1.9 mol) and nitric acid (0.1 mol) were mixed in the beakers, which were stirred for 30 min and labeled as A solution; a requisite amount of butyl titanate (0.1 mol) were stirred in anhydrous ethanol (2.3 mol) for 30 min and labeled as B solution; then B solution was added drop-wisely to A solution with vigorous stirring. After stirring for 5 h at room temperature, the sol was concentrated in 40 °C water bath and subsequently dried at 80 °C for 24 h. The gel was calcinated at 500 °C for 5 h in air. TiO_2–CeO_2 composite oxide carriers was denoted as $TiCe_a$ ("a" represents the CeO_2/TiO_2 mass ratio; a = 0.11, 0.25, 0.43, 0.67, 1.00).

Stoichiometric amount of ammonium wolframate solution and ammonium metavanadate were mixed in the oxalic solution of desired proportions, which was labeled as C solution. V_2O_5–WO_3/TiO_2–CeO_2 catalysts were prepared by the dispersal of a certain mass of $TiCe_a$ powder into 50 ml C solution at 80 °C to obtain the slurry. The slurry was stirred for 2 h, after that, the mixture was exposed to an ultrasonic bath for 2 h, dried at 105 °C for 12 h and subsequently calcined at 500 °C for 3 h in air. Finally, CeO_2 doped catalyst V_2O_5–WO_3/TiO_2 was obtained and abbreviated as V_xWTiCe_a ("x" represents the V_2O_5/(V_2O_5 + WO_3 + TiO_2 + CeO_2) mass ratio, $x = 0.40 \times 10^{-2}$, 0.60×10^{-2}, 0.80×10^{-2}, 1.00×10^{-2}, 1.20×10^{-2}). Meanwhile, WO_3/TiO_2 (WTi) catalysts, V_2O_5–WO_3/TiO_2 (VWTi) catalysts and WO_3/TiO_2–CeO_2 (WTiCe) catalysts were synthesized by impregnation method, and the processes were the same as the foregoing conditions. The mass loading of WO_3 on all catalysts was 8%.

2.3. Catalytic activity measurement

The experimental setup for evaluating Hg^0 oxidation on the samples was shown in Fig. 1. The catalytic activities of Hg^0 oxidation were tested at 80–350 °C in a fixed bed reactor under atmospheric pressure. The reaction temperature was controlled by a digital temperature controller. 0.5 g catalyst samples were packed in the center of the quartz tube (i. d. 20 mm). The simulated flue gas (SFG) was consisted of 70.00 μg/m^3 Hg^0, 500 ppm SO_2 (20.4% SO_2 + 79.6% N_2), 1000 ppm NO (20.0% NO + 80.0%N_2), 12%CO_2 (99.999%), 5% O_2 (99.999%) and balanced gas N_2 (99.999%). The feed gas was controlled by mass flow meters and injected into the reactor at a total rate of 1 L min^{-1} with a gas hourly space velocity of 1.0×10^5 h^{-1}. A constant quantity of Hg^0 vapor was supplied into the gas steam, with an Hg^0 permeation tube (VICI Metronics, USA) which was immersed in a water bath. A peristaltic pump transferred water into the Teflon tube wrapped with a

temperature-controlled heating tape and then water vapor was generated. 100 ml pure N_2 took the water vapor along and mixed with the flue gas. Besides, In order to avoid adsorption of Hg^0 and condensation of water vapor on the inner surface, all Teflon lines that Hg^0 and H_2O (g) passed through were heated up to 120 °C. The Hg^0 concentration in the inlet and outlet gas was online measured by a RA-915 M Mercury Analyzer (LUMEX Ltd, Russia) which can measure solely the concentration of Hg^0. Meanwhile, Hg^0 concentration was recorded after the process had reached equilibrium. The time was more than 2 h. The experiment was carried out to ensure the reliability of data obtained from the test on catalyst performance. Result showed that VWTiCe catalyst possessed excellent stability on Hg^0 oxidation and could perform well in presupposed time quantum of 2 h for experiment. Water vapor was removed by the condenser before proceeding to the mercury analyzer.

Before the test, the flue gas bypassed the reactor and Hg^0 concentration in the inlet ($[Hg^0]_{in}$) was measured. Then, the gas flow was switched to pass through the catalysts and Hg^0 concentration in the outlet ($[Hg^0]_{out}$) was measured. The loss of Hg^0 concentration over the catalysts should be due to the oxidation or adsorption of Hg^0. In order to avoid possible bias because of Hg^0 adsorption, at the beginning of the Hg^0 catalytic oxidation tests, the catalysts were first saturated with the established $[Hg^0]_{in}$ under N_2 atmosphere at room temperature [23,33,37]. The adsorption test result indicated that the capacities of catalyst samples to adsorb Hg^0 were negligible at room temperature. Therefore, Hg^0 oxidation efficiency (E_{oxi}) over the catalysts was quantified by the following equation:

$$E_{oxi}(\%) = \frac{[Hg^0]_{in} - [Hg^0]_{out}}{[Hg^0]_{in}} \times 100\% \quad (1)$$

2.4. Characterization

Brunauer–Emmett–Teller (BET) surface area, average pore size, and average pore volume of the samples were analyzed by Micromeritics Tristar II 3020 analyzer (Micromeritics Instrument Crop, USA). Each sample was degassed in vacuum at 180 °C for 5 h. The specific surface areas were calculated by the BET method. The average pore diameter and average pore volume were obtained from the desorption branches of N_2 adsorption isotherm and calculated by the BJH (Barrett–Joyner–Halenda) formula.

X-ray diffractogram (XRD) measurements were carried out on Rigaku rotaflex D/Max-C powder diffractometer (Rigaku, Japan) to examine the crystallinity and dispersivity of each species on the support. The XRD patterns were used nickel-filtered Cu Kα radiation (λ = 0.1543 nm) in the range of 10–80° (2θ) with a step size of 0.02°.

X-ray Photoelectron Spectroscopy (XPS) analysis was carried out at room temperature on a K-Alpha 1063 X-ray photoelectron spectrometer (Thermo Fisher Scientific, UK) with an Al Kα X-ray source. The observed spectra were calibrated with the C 1s binding energy (BE) value of 284.6 eV.

3. Results and discussion

3.1. Catalytic activity tests

The comparison of catalytic performance of different catalysts as a function of temperature from 80 to 350 °C was shown in Fig. 2. E_{oxi} over WTi was below 40% in the entire temperature range. On the $TiCe_{0.25}$ catalyst, E_{oxi} increased with temperature from 80 to 250 °C, and then decreased when temperature further increased from 250 to 350 °C. $V_{0.80}WTiCe_{0.25}$ performed the best mercury oxidation and approximately 88.93% mercury oxidation efficiency was obtained at 250 °C. Additionally, it was clearly found that the addition of ceria noticeably expanded the active temperature window and also improved the catalytic performance on Hg^0 oxidation. In the whole temperature range, E_{oxi} over $V_{0.80}WTiCe_{0.25}$ was higher than that over $WTiCe_{0.25}$, $V_{0.80}WTi$ and $TiCe_{0.25}$ catalyst. This result demonstrated that the combination of CeO_2 and V_2O_5 resulted in significant synergy for Hg^0 oxidation.

The effect of CeO_2 modified on the performance of $V_{0.80}WTiCe_a$ was displayed in Fig. 3. The addition of CeO_2 significantly enhanced

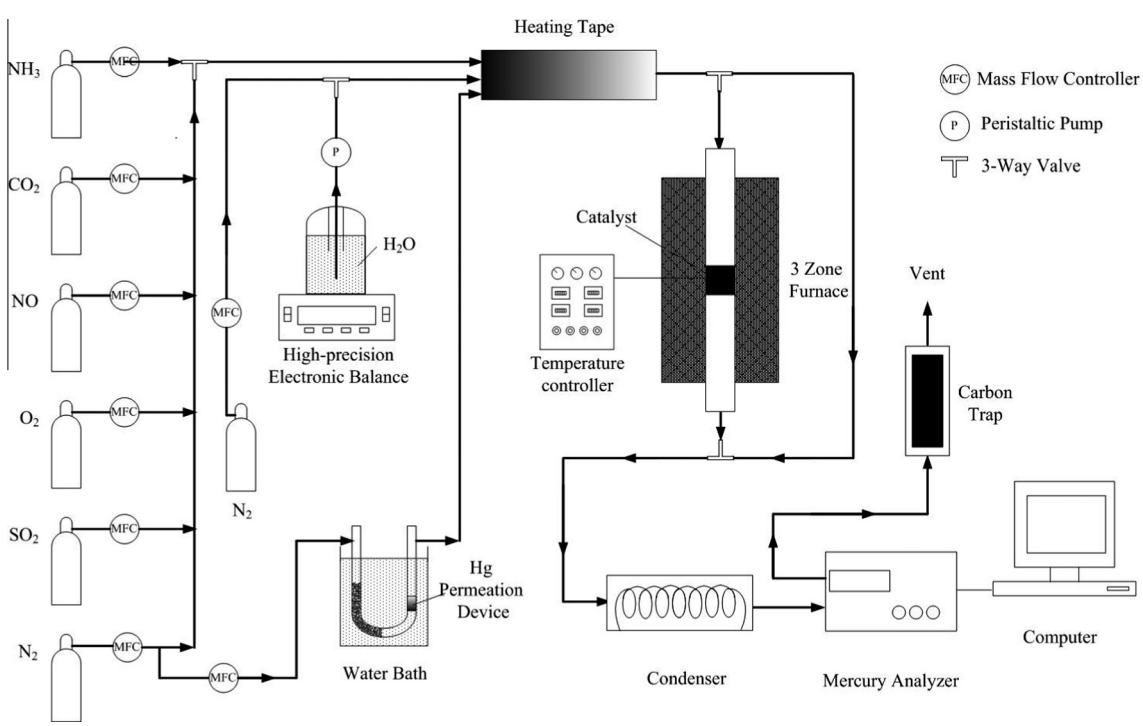

Fig. 1. Schematic diagram of the experimental setup.

the mercury oxidation activity of $V_{0.80}WTiCe_a$. For instance, E_{oxi} of $V_{0.80}WTi$ was only 42.59%, while the minimal E_{oxi} still had 65.10% over $V_{0.80}WTiCe_a$. Moreover, Catalyst with a CeO_2/TiO_2 mass ratio of 0.25 performed the best activity and 88.93% mercury oxidation efficiency was obtained. However, further increase of CeO_2/TiO_2 mass ratio, Hg^0 oxidation efficiency would be weakened. Accordingly, the optimal CeO_2/TiO_2 mass ratio was about 0.25.

To investigate the synergetic interaction between V_2O_5 and CeO_2, the effect of various V_2O_5 loading from on the performance of $V_xWTiCe_{0.25}$ was also studied, and the results were depicted in Fig. 4. For all $V_xWTiCe_{0.25}$, E_{oxi} increased with temperature from 80 to 250 °C and then decreased when temperature further increased. In the temperature range (250–350 °C), increase of V_2O_5 loading yielded more Hg^0 oxidation. This illustrated that the V_2O_5-rich catalyst showed superior activity. However, activity difference between $V_{0.80}WTiCe_{0.25}$ and $V_{1.00}WTiCe_{0.25}$ was relatively small in comparison with that of other catalysts at 250 °C. Besides, $V_{1.00}WTiCe_{0.25}$ showed almost the same activity as $V_{1.20}WTiCe_{0.25}$ at 200 °C. It is worth noting that $V_{0.80}WTiCe_{0.25}$ displayed excellent performance for Hg^0 oxidation with temperature from 80 to 150 °C. According to the literature [38], CeO_2 was active for Hg^0 oxidation at low temperature. Above results demonstrated that Hg^0 oxidation activities of $V_xWTiCe_{0.25}$ were aided by synergistic effect between V_2O_5 and CeO_2.

3.2. Characterization of $V_{0.80}WTiCe_{0.25}$

3.2.1. Analysis of specific area (BET) and XRD patterns

The BET surface area, BJH pore volume and average pore volume of different samples were summarized in Table 1. From the table, $WTiCe_{0.25}$ and $V_{0.80}WTiCe_{0.25}$ exhibited higher specific surface areas. The introduction of CeO_2 increased the surface area and pore volume but lowered the average pore diameter (Fig. 5a). The results suggested the addition of CeO_2 was beneficial to the specific area accretion. The high specific surface area of the TiO_2–CeO_2 composite oxides was due to the amorphous structure that the oxides formed through the sol–gel procedure [38]. Furthermore, as the impregnation of V_2O_5, the specific surface area and pore volume of $V_{0.80}WTiCe_{0.25}$ decreased. It might be caused by deposited active oxides, which penetrated into the pores of the support. In addition, as displayed in Fig. 5b and c, for $V_{0.80}WTiCe_{0.25}$, there was significant hysteresis between adsorption and desorption isotherms, which is usually an indication of mesoporous materials. This clarified that the mesoporous structure was formed by aggregation of nano-particles. This structure might facilitate mass transfer in the catalytic reaction [29].

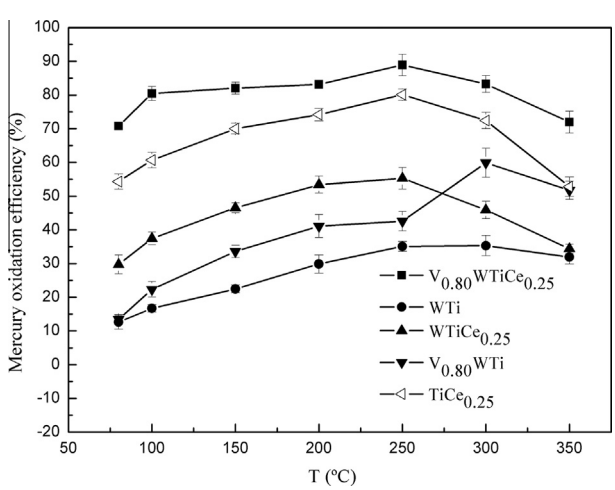

Fig. 2. Comparison of catalytic performance of different catalysts. Reaction conditions: 1000 ppm NO, 500 ppm SO_2, 5% O_2, 12% CO_2, N_2 as balance gas.

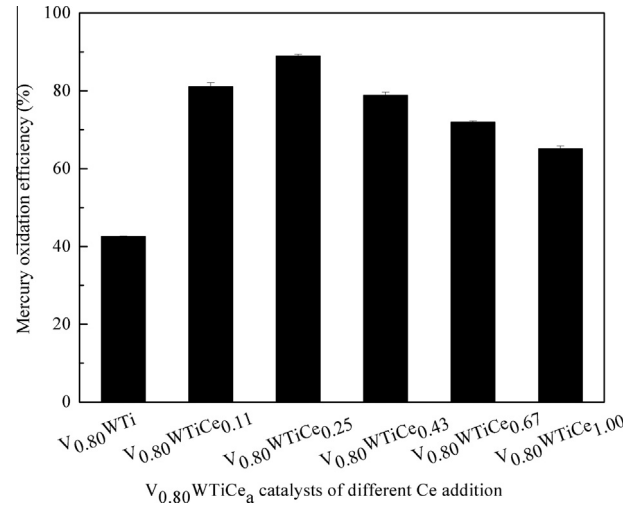

Fig. 3. Effect of CeO_2 modified on the performance of $V_{0.80}WTiCe_a$. Reaction conditions: 1000 ppm NO, 500 ppm SO_2, 5% O_2, 12% CO_2, N_2 as balance gas.

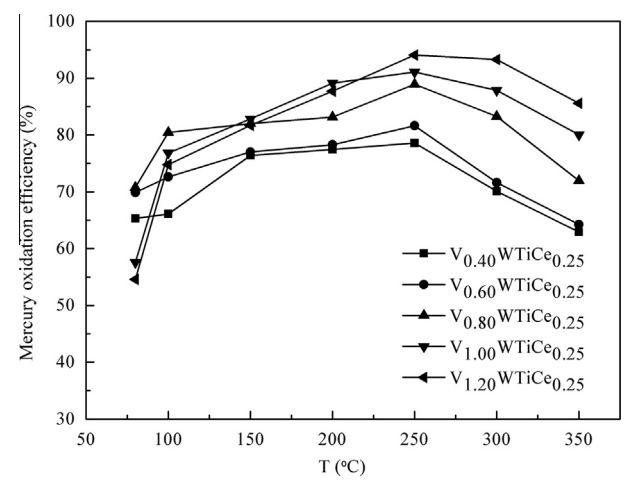

Fig. 4. Effect of $V_xWTiCe_{0.25}$ catalysts of various V loadings. Reaction conditions: 1000 ppm NO, 500 ppm SO_2, 5% O_2, 12% CO_2, N_2 as balance gas.

The XRD patterns of the catalysts were displayed in Fig. 6. The characteristic peaks of V_2O_5 and WO_3 could be hardly detected for all catalysts, which were due to the widely dispersion and poorer crystalline on the surface. From the XRD figure, it can be seen that the diffraction peaks of WTi and $V_{0.80}WTi$ showed typical anatase-phase TiO_2. The diffraction line of WTi and $V_{0.80}WTi$ were narrow and sharp, which indicated the formation of large TiO_2 crystal particles [38]. In the pattern of the $WTiCe_{0.25}$ and $V_{0.80}WTiCe_{0.25}$, only the broadened diffraction peak of anatase-phase TiO_2 was observed. It also can be seen that the height of half-peak breadth of TiO_2 on

Table 1
The surface area, pore volume and pore diameter of the samples.

Catalysts	BET surface area (m^2/g)	Pore volume (cm^3/g)	Average pore diameter (nm)
WTi	38.4855	0.1322	13.7379
$V_{0.80}WTi$	41.6403	0.1432	13.7511
$WTiCe_{0.25}$	122.9062	0.2931	9.5404
$V_{0.80}WTiCe_{0.25}$	116.6715	0.2809	9.6293

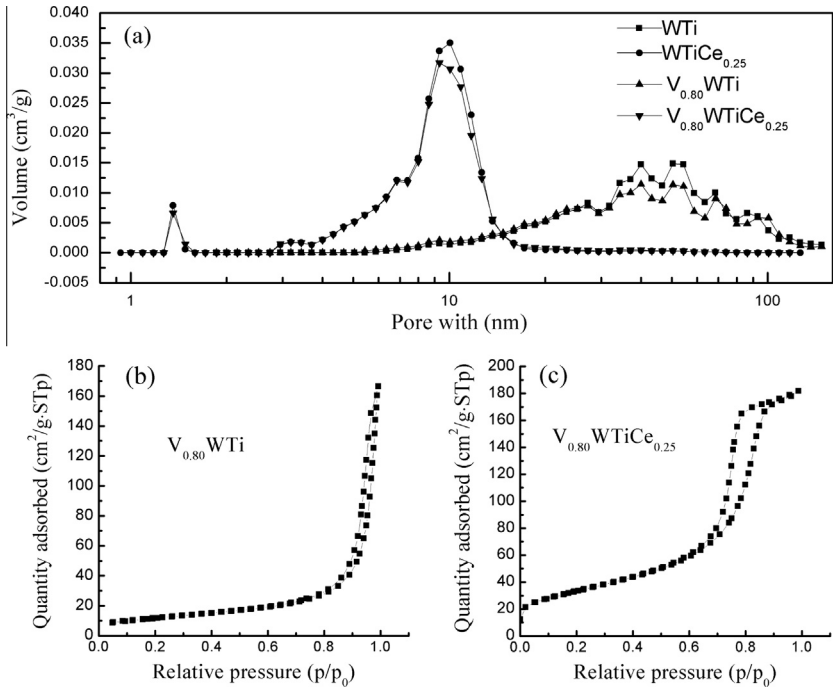

Fig. 5. Physical properties of different catalysts. (a) Particle size distribution of WTi, $V_{0.80}$WTi, $WTiCe_{0.25}$ and $V_{0.80}WTiCe_{0.25}$; (b) N_2 adsorption and desorption isotherms of $WTiCe_{0.25}$; (c) N_2 adsorption and desorption isotherms of $V_{0.80}WTiCe_{0.25}$.

$WTiCe_{0.25}$ and $V_{0.80}WTiCe_{0.25}$ were much lower than that on WTi and $V_{0.80}$WTi. This revealed that the crystal particle of TiO_2 on $WTiCe_{0.25}$ and $V_{0.80}WTiCe_{0.25}$ were much smaller than that on WTi and $V_{0.80}$WTi. Moreover, cubic CeO_2 was not observed in $WTiCe_{0.25}$ and $V_{0.80}WTiCe_{0.25}$. This demonstrated that CeO_2 probably only contained amorphous phase or crystallite phase with very small particle size [31].

Thus, according to the BET and XRD results, the addition of an appropriate amount of CeO_2 was beneficial not only for the formation of the TiO_2 crystal phase but also for the dispersion of active sites over the carrier. Besides, high concentration of amorphous or highly dispersed crystalline CeO_2 should be a rational reason for the excellent performance of the $V_{0.80}WTiCe_{0.25}$.

3.2.2. Element valences of $V_{0.80}WTiCe_{0.25}$

To determine the oxidation states of the element in these materials and to get a better understanding nature of the interactions in the catalyst system, the catalysts were investigated by XPS technique. The XPS spectra for O 1s for fresh WTi, $WTiCe_{0.25}$, $V_{0.80}$WTi and $V_{0.80}WTiCe_{0.25}$ were shown in Fig. 7. It could be seen that the introduction of CeO_2 increased the binging energy of O. The peak appeared at low binding energy (529.5–530.0 eV) could be assigned to be the lattice oxygen (denoted as O_β) [39], while the binding energy of 531.0–531.6 eV was assigned to the chemisorbed oxygen (denoted as O_α), such as O^{2-} and O^- belonging to defect oxide or hydroxyl like group [40]. O_α was often thought to be the most active oxygen and played an important role in oxidation reaction [41,42]. In this study O_α ratio of $WTiCe_{0.25}$ (42.63%), calculated by $O_\alpha/(O_\alpha + O_\beta)$, was higher than that of WTi (33.21%), which meant that CeO_2 was helpful for mercury oxidation. CeO_2 was easy to form labile oxygen vacancies and particularly the relatively high mobility of bulk oxygen species, which may conduce to the improvement of chemisorbed oxygen [43]. Moreover, O_α ratio of $V_{0.80}WTiCe_{0.25}$ (48.32%) was higher than that of $WTiCe_{0.25}$ (42.63%) and $V_{0.80}$WTi (41.19%). This result meant that there was synergistic effect between V_2O_5 and CeO_2, which resulted in more surface oxygen vacancies. It also meant that $V_{0.80}WTiCe_{0.25}$ might have better activity for mercury oxidation than WTi, $WTiCe_{0.25}$ and $V_{0.80}$WTi. Thus, the addition of CeO_2 has a positive effect on mercury oxidation reaction. This conclusion was in good agreement with the results of the activity tests for these catalysts.

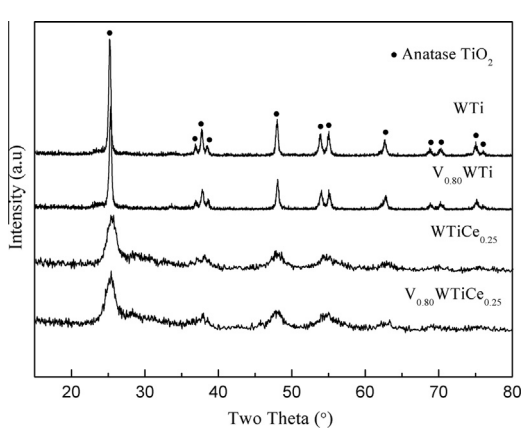

Fig. 6. XRD patterns of WTi, $V_{0.80}$WTi, $WTiCe_{0.25}$ and $V_{0.80}WTiCe_{0.25}$.

The Ce 3d spectra of fresh $V_{0.80}WTiCe_{0.25}$ and spent $V_{0.80}WTiCe_{0.25}$ investigated in this study were presented in Fig. 8. The bands labeled u^1 and v^1 represent the $3d^{10}4f^1$ initial electronic state, corresponding to Ce^{3+}, whereas the peaks labeled u, u^2, u^3, v, v^2, and v^3 represent the $3d^{10}4f^0$ state of Ce^{4+} ions [44]. It could be clearly seen the high ratio of Ce^{3+} (40.27%) over fresh $V_{0.80}WTiCe_{0.25}$. In comparison with the fresh sample, the ratio of Ce^{3+} increased to 43.82% on spent $V_{0.80}WTiCe_{0.25}$. This implied that the conversion from Ce^{4+} to Ce^{3+} was predominant within the redox shift between Ce^{3+} and Ce^{4+}. Within the redox shift, labile oxygen vacancies and bulk oxygen species with relatively high

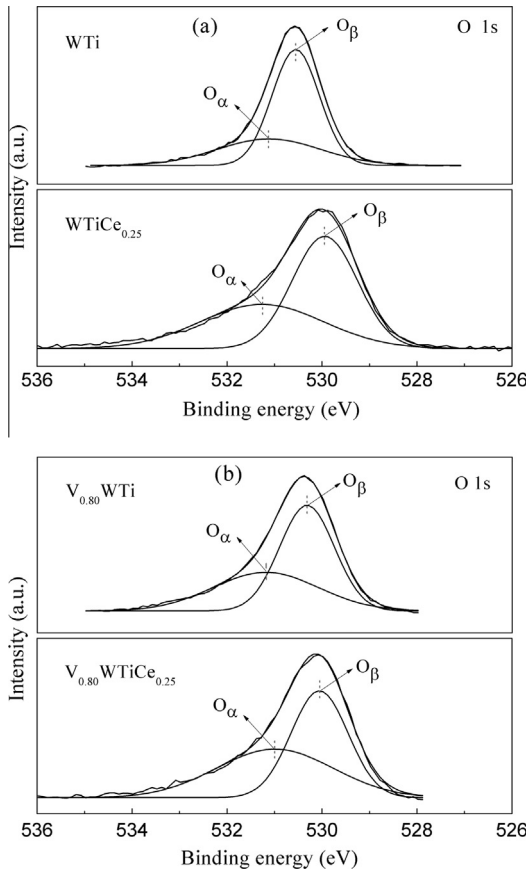

Fig. 7. O_{1s} XPS spectra for WTi, $V_{0.80}$WTi, $WTiCe_{0.25}$ and $V_{0.80}WTiCe_{0.25}$.

mobility could be easily generated [43]. Furthermore, it was reported that the lattice oxygen defects over catalyst surface would be improved by increasing the content of Ce^{3+}, which improved the redox transformation between Ce^{3+} and Ce^{4+} [45]. Meanwhile, two peaks at binding energy of 517.2 eV and 515.9 eV for the fresh $V_{0.80}WTiCe_{0.25}$ (Fig. 9) represented V_2O_4 species with V^{4+} and V_2O_5 species with V^{5+}, respectively [46,47]. However, only V^{5+} was detected on spent $V_{0.80}WTiCe_{0.25}$. It was assumed that V^{4+} could be oxidized to V^{5+} over the sample. This phenomenon implied V_2O_4 and CeO_2 were in a partially reduced state on the surface of catalyst, which might be attributable to the presence of strong interactions between V_2O_4 and CeO_2. It was most likely that V^{4+} could be oxidized to V^{5+}, which was benefited from the transformation from Ce^{4+} to Ce^{3+} ions.

The Hg 4f spectra of spent $V_{0.80}WTiCe_{0.25}$ and spent $V_{0.80}WTiCe_{0.25}$ were presented in Fig. 10. The Hg 4f spectrum of spent $V_{0.80}WTiCe_{0.25}$ exhibited contributions from two components. According to the reported binding energies for Hg 4f on reference [48], the components can be ascribed to Hg^0 and HgO with two peaks locating at 102.6 eV and 108.5 eV, respectively. Therefore, the XPS peak intensities and binding energies of Hg 4f line indicated that mercury was present as Hg^0 and HgO on the spent $V_{0.80}WTiCe_{0.25}$. It was concluded that Hg^0 was firstly adsorbed onto the active sites of the catalyst, and subsequently oxidized to HgO. It was very likely that Hg^0 oxidation of $V_{0.80}WTiCe_{0.25}$ could be mainly influenced by the O species on the samples surface. However, the absence of peaks for Hg adsorbed over the $V_{0.80}$WTi indicated that the concentration of Hg adsorbed was below the capabilities of XPS equipment detection or the adsorbed Hg desorbed from the surface of catalyst. This results confirmed that CeO_2 modified $V_{0.80}$WTi might have better activity for the adsorption and oxidation of Hg^0 than unmodified $V_{0.80}$WTi. In other words, the addition of CeO_2 not only improved the oxygen storage, but also enhanced the redox activity through the interaction between V_2O_5 and CeO_2.

3.3. Effect of flue gas constituents on Hg^0 oxidation

To explore the roles of individual flue gas components in Hg^0 oxidation, the effects of reactant gas composition on activity were studied. The experimental conditions are listed in Table 2. Experiments were conducted at 250 °C, by individual flue gas components balanced in pure N_2 and/or in combination with O_2. The results were shown in Fig. 11.

3.3.1. Effect of O_2

O_2 promoted Hg^0 oxidation. In pure N_2 gas flow, E_{oxi} was low which should be due to gas-phase or weakly adsorbed Hg^0 reacting with lattice oxygen to form mercuric oxide [49]. Nevertheless, E_{oxi} increased from 41.98% to 71.13% when 5% O_2 was added to the gas flow. Obvious increase of E_{oxi} was detected when O_2 concentration further increased to 10% as well. It has been reported that lattice oxygen of the metal oxides can serve as the oxidant of Hg, forming mercuric oxide (HgO) [50]. E_{oxi} was low may be attributed to the consumption of the lattice oxygen. O_2 (g) can replenish the consumed chemisorbed oxygen and regenerate the lattice oxygen,

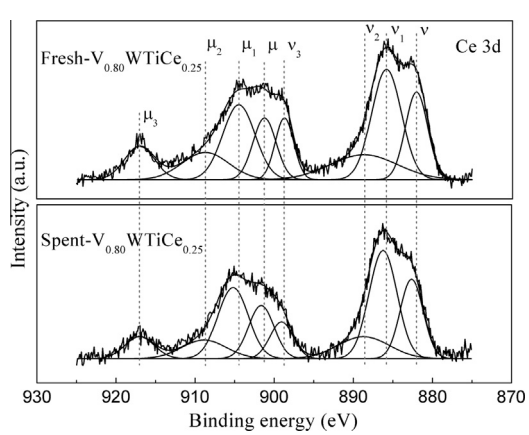

Fig. 8. Ce_{3d} XPS spectra for fresh – $V_{0.80}WTiCe_{0.25}$ and spent – $V_{0.80}WTiCe_{0.25}$ (the sample was subjected to Hg^0 oxidation under simulated flue gas with the temperature of 250 °C).

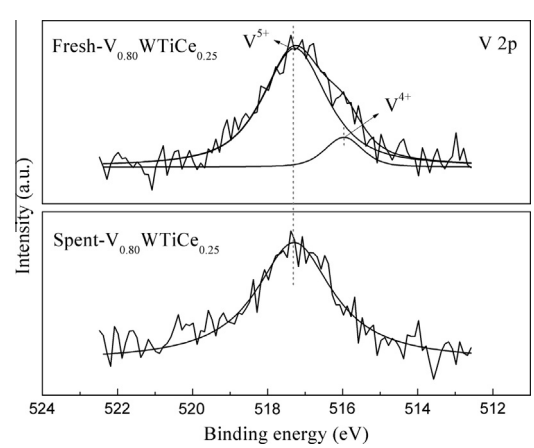

Fig. 9. V_{2P} XPS spectra for fresh – $V_{0.80}WTiCe_{0.25}$ and spent – $V_{0.80}WTiCe_{0.25}$ (the sample was subjected to Hg^0 oxidation under simulated flue gas with the temperature of 250 °C).

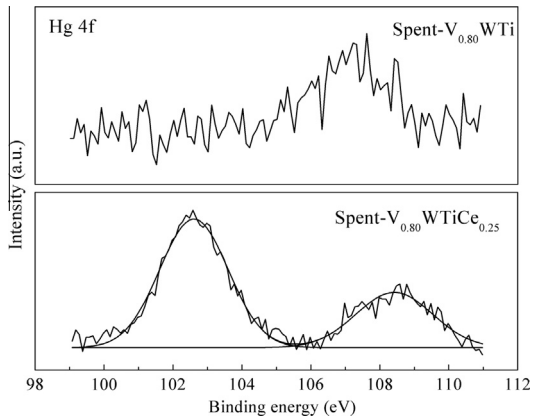

Fig. 10. Hg_{4f} XPS spectra for spent – $V_{0.80}WTiCe_{0.25}$ and spent – $V_{0.80}WTiCe_{0.25}$ (the sample was subjected to Hg^0 oxidation under simulated flue gas with the temperature of 250 °C).

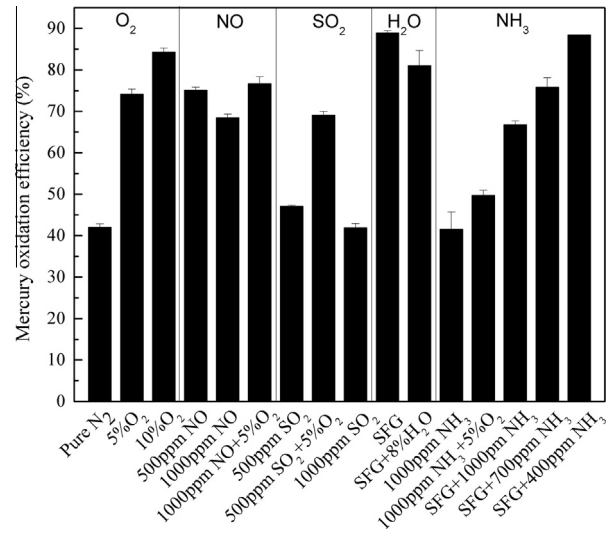

Fig. 11. Effects of individual flue gas components on Hg^0 oxidation of $V_{0.80}WTiCe_{0.25}$.

which serves as the Hg^0 oxidant [37]. Hence, obvious increase of Hg^0 oxidation efficiency was detected when 5% O_2 (g) was introduced to the pure N_2 carrier gas or even when O_2 (g) concentration further increased to 10%.

3.3.2. Effect of NO

Addition of 500 ppm NO has an enhancing effect on Hg^0 oxidation under pure N_2 atmosphere. Compared to the results obtained under N_2 atmosphere, the oxidation Hg^0 concentration was higher when NO was present in the reactor. This may be due to the addition of CeO_2 in the catalyst which can adsorb and oxidation NO. Jin et al. [51] found that a fraction of NO reacted with the surface oxygen to form NO_x species, which could enhance Hg^0 oxidation [49]. However, the addition of 1000 ppm NO into pure N_2 resulted in a slight decrease of E_{oxi} from 75.10% to 68.42%. Nonetheless, adding 5% O_2 and 1000 ppm NO to the flow gas improved the catalytic performance. It was hypothesized that lattice oxygen might participate in NO oxidation. The reaction consumed surface oxygen which resulted in a slight decrease of Hg^0 oxidation at 1000 ppm NO. Hg^0 oxidation would be increased once surface oxygen was enough for NO and Hg^0 oxidation. Therefore, NO has a promotional effect on Hg^0 oxidation in the presence of O_2.

3.3.3. Effect of SO_2

The addition of 500 ppm SO_2 slightly promoted the Hg^0 oxidation efficiency. 500 ppm SO_2 added to gas stream with O_2 (g) also enhanced the catalytic activity. This indicated that promotional effect of SO_2 on Hg^0 oxidation was obtained with the aid of O_2 (g). However, the addition of 1000 ppm SO_2 into pure N_2 resulted in a slight decrease of E_{oxi} from 47.04% to 41.85%. It was very likely that SO_2 reacted with the surface oxygen to form SO_3 [52]. The reaction consumed the reactive oxygen which was active for Hg^0 oxidation in the pure N_2 [53]. Thus, the inhibitive effect of SO_2 would be obviously reduced by the addition of O_2 (g). These behaviors were well consistent with the literature results [54].

Table 2
Experimental conditions.

Experiments	Catalysts	Flue gas components (1 L min^{-1})
Set I	$V_{0.80}WTiCe_{0.25}$	N_2
		N_2 + 5% O_2
		N_2 + 10% O_2
Set II		N_2 + 500 ppm NO
		N_2 + 1000 ppm NO
		N_2 + 1000 ppm NO + 5% O_2
Set III		N_2 + 500 ppm SO_2
		N_2 + 1000 ppm SO_2
		N_2 + 500 ppm SO_2 + 5% O_2
Set IV		SFG:N_2 + 1000 ppm NO + 500 ppm SO_2 + 12% CO_2 + 5% O_2
		SFG + 8% H_2O
Set V		N_2 + 1000 ppm NH_3
		N_2 + 1000 ppm NH_3 + 5% O_2
		SFG + 400 ppm NH_3
		SFG + 700 ppm NH_3
		SFG + 1000 ppm NH_3

3.3.4. Effect of H_2O

H_2O inhibited Hg^0 oxidation over the $V_{0.80}WTiCe_{0.25}$ due to competitive adsorption, which was consistent with the values reported in the literature [33]. However, compared with the previous research [28], the reduction of E_{oxi} over the $V_{0.80}WTiCe_{0.25}$ was minor. This result implied that the $V_{0.80}WTiCe_{0.25}$ exhibited good resistance to H_2O.

3.3.5. Effect of NH_3

As a SCR catalyst, $V_{0.80}WTiCe_{0.25}$ would probably be used under SCR conditions where NH_3 is usually present. Hence, it is necessary to study the effect of NH_3 on the oxidation of Hg^0. 1000 ppm NH_3 was added to pure N_2 atmosphere. NH_3 concentration had a slight influence on E_{oxi}: the efficiency was 49.70% at 1000 ppm NH_3 plus 5% O_2 atmosphere which was slightly higher than that under 1000 ppm NH_3 without O_2. According to the previous study, NH_3 consumed the surface oxygen that is responsible for Hg^0 oxidation [55]. Gaseous NH_3 are adsorbed on the catalyst surface to form coordinated NH_3 and NH_2. The possible reactions over VWTiCe are proposed to be as follows:

$$NH_{3(g)} \rightarrow NH_{3(ad)} \quad (2)$$

$$NH_{3(ad)} + O^* \rightarrow NH_{2(ad)} + OH_{(ad)} \quad (3)$$

where O^* are active surface oxygen of the catalyst. However, many researchers have confirmed that there is a competitive adsorption between NH_3 and Hg^0. Therefore, the competitive adsorption of NH_3 and Hg^0 on the VWTiCe catalyst was investigated by a desorption experiment, the results are shown in Fig. 12. $V_{0.80}WTiCe_{0.25}$ saturated by Hg^0 at 250 °C under a flow of Hg^0 balanced in N_2 was used in this test. From the figure, no obvious increase in the Hg^0 concentration was observed after adding 1000 ppm NH_3 and

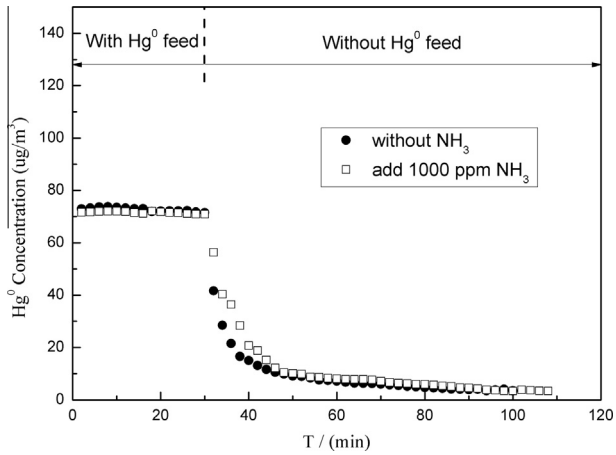

Fig. 12. Desorption of Hg^0 from $V_{0.80}WTiCe_{0.25}$ by NH_3.

turning off the Hg^0 at the same time. The result demonstrates that NH_3 cannot inhibit Hg^0 adsorption onto the active sites.

Besides, E_{oxi} under SCR atmosphere was also investigated. The SCR atmosphere was defined as SFG plus NH_3, with the NH_3/NO ratio of 1. When 1000 ppm NH_3 was introduced into the SFG to make SCR atmosphere, E_{oxi} decreased from 88.93% to 66.78%. This illustrated that the presence of NH_3 inhibited Hg^0 removal over the $V_{0.80}WTiCe_{0.25}$ catalyst. However, the E_{oxi} significantly increased with the decrease of NH_3/NO ratio. As already mentioned, NO had a promotional effect on Hg^0 oxidation over $V_{0.80}WTiCe_{0.25}$ in the presence of O_2. It should be noted that the SCR reaction consumed NO and O_2. Thus, it would be deduced that the concentrations of NO and O_2 would increase with the decrease of NH_3/NO ratio as the SCR reaction occurred simultaneously with Hg^0 oxidation. In another words, there would be more available surface oxygen for NO promoting the oxidation of Hg^0 with the decrease of NH_3/NO ratio. Nevertheless, the E_{oxi} of 66.78% is still encouraging, since lower space velocity and the typical flue gas with HCl would result in higher Hg^0 oxidation efficiency.

3.4. Mechanism

From the results above, the catalysis mechanism for Hg^0 oxidation can be explained by the Mars–Maessen mechanism. In this mechanism, adsorbed Hg^0 would react with a lattice oxidant of catalyst (either O or Cl) that is replenished from the gas phase [10,56]. The active oxygen atom could produce by breaking O–O bonds on the surface of V_2O_5, then $Hg^0_{(ad)}$ molecular could pick up the dissociated O atom and forming HgO. This explains why E_{oxi} gradually increased as O_2 concentration increased. The possible mechanism for enhanced Hg^0 oxidation could be explained by the following reactions:

$$Hg^0_{(g)} + \text{surface} \rightarrow Hg^0_{(ad)} \quad (4)$$

$$Hg^0_{(ad)} + V_2O_5 \rightarrow HgO_{(ad)} + V_2O_4 \quad (5)$$

$$HgO_{(ad)} \rightarrow HgO_{(g)} \quad (6)$$

$$V_2O_4 + 2CeO_2 \rightarrow V_2O_5 + Ce_2O_3 \quad (7)$$

$$Ce_2O_3 + \frac{1}{2}O_{2(g)} \rightarrow 2CeO_2 \quad (8)$$

The overall reactions can be summarized as follows:

$$Hg^0_{(g)} + \frac{1}{2}O_{2(g)} \rightarrow HgO_{(g)} \quad (9)$$

Gaseous Hg^0 was firstly adsorbed onto the active sites of catalyst to form $Hg^0_{(ad)}$; and then the catalytic reaction is losing one oxygen atom from V_2O_5 to $Hg^0_{(ad)}$ to form HgO. The consumption of V_2O_5 could be compensated by V_2O_4 bond with CeO_2. Finally, the missing lattice oxygen of CeO_2 would be replaced by oxygen from the flue gas. The redox couples of V^{4+}/V^{5+} seems to play an important role for mercury oxidation to proceed. CeO_2 contains many lattice oxygen species on the surface because of the cerium in CeO_2 can easily occupy two oxidation states [CeO_2 (Ce^{4+}) $\leftrightarrow$ Ce_2O_3 (Ce^{3+})]. Consequently, CeO_2 can contribute to the redox process of V^{4+}/V^{5+}. It provided lattice oxygen to V_2O_5 to increase the valence and oxidation ability of V_2O_5.

4. Conclusions

The CeO_2 modified VWTi displayed excellent performance for Hg^0 oxidation. Hg^0 oxidation could be improved by the addition of CeO_2 and $V_{0.80}WTiCe_{0.25}$ showed the best mercury oxidation efficiency in simulated coal-fired flue gas at 250 °C. NO and SO_2 were observed to promote Hg^0 removal with the presence of O_2. The catalyst exhibited good resistance to H_2O. Besides, the activity of catalysts for Hg^0 oxidation decreased with the presence of NH_3. Furthermore, the high activity of catalyst might ascribe to synergistic effect between V_2O_5 and CeO_2. A likely reaction pathway for Hg^0 oxidation on $V_{0.80}WTiCe_{0.25}$ was Mars–Maessen mechanism, where lattice oxygen of V_2O_5 reacts with adjacently absorbed Hg^0. Being a novel SCR catalyst with higher Hg^0 oxidation efficiency, further investigations will be to examine the performance of catalysts for simultaneous NO_x and Hg^0 removal without HCl.

Acknowledgments

This work was financially supported by the National Natural Science Foundation of China (51278177, 51478173), and the National High Technology Research and Development Program of China (863 Program, No. 2011AA060803).

References

[1] Lee W, Bae GN. Removal of elemental mercury (Hg (0)) by nanosized V_2O_5/TiO_2 catalysts. Environ Sci Technol 2009;43(5):1522–7.
[2] Li J, Yan N, Qu Z, Qiao S, Yang S, Guo Y, et al. Catalytic oxidation of elemental mercury over the modified catalyst Mn/α-Al_2O_3 at lower temperatures. Environ Sci Technol 2009;44(1):426–31.
[3] Xu W, Wang H, Zhu T, Kuang J, Jing P. Mercury removal from coal combustion flue gas by modified fly ash. J Environ Sci 2013;25(2):393–8.
[4] Pirrone N, Cinnirella S, Feng X, Finkelman RB, Friedli HR, Leaner J, et al. Global mercury emissions to the atmosphere from anthropogenic and natural sources. Atmos Chem Phys 2010;10(13):5951–64.
[5] Auzmendi-Murua I, Castillo Á, Bozzelli JW. Mercury oxidation via chlorine, bromine, and iodine under atmospheric conditions: thermochemistry and kinetics. J Phys Chem A 2014;118(16):2959–75.
[6] Zheng Y, Jensen AD, Windelin C, Jensen F. Dynamic measurement of mercury adsorption and oxidation on activated carbon in simulated cement kiln flue gas. Fuel 2012;93:649–57.
[7] Li JR, He C, Shang XS, Chen JS, Yu XW, Yao YJ. Oxidation efficiency of elemental mercury in flue gas by SCR De-NO_x catalysts. J Fuel Chem Technol 2012;40(2):241–6.
[8] McLarnon CR, Granite EJ, Pennline HW. The PCO process for photochemical removal of mercury from flue gas. Fuel Process Technol 2005;87(1):85–9.
[9] Zhuang Y, Thompson JS, Zygarlicke CJ, Pavlish JH. Development of a mercury transformation model in coal combustion flue gas. Environ Sci Technol 2004;38(21):5803–8.
[10] Presto AA, Granite EJ. Survey of catalysts for oxidation of mercury in flue gas. Environ Sci Technol 2006;40(18):5601–9.
[11] Granite EJ, Myers CR, King WP, Stanko DC, Pennline HW. Sorbents for mercury capture from fuel gas with application to gasification systems. Ind Eng Chem Res 2006;45(13):4844–8.
[12] Hsi HC, Lee HH, Hwang JF, Chen W. Mercury speciation and distribution in a 660-Megawatt utility boiler in taiwan firing bituminous coals. J Air Waste Manage 2010;60(5):514–22.
[13] Wiatros-Motyka MM, Sun CG, Stevens LA, Snape CE. High capacity co-precipitated manganese oxides sorbents for oxidative mercury capture. Fuel 2013;109:559–62.

[14] Sun C, Snape CE, Liu H. Development of low-cost functional adsorbents for control of mercury (Hg) emissions from coal combustion. Energy Fuel 2013;27(7):3875–82.
[15] Wang YJ, Liu Y, Wu ZB, Mo JS, Cheng B. Experimental study on the absorption behaviors of gas phase bivalent mercury in Ca-based wet flue gas desulfurization slurry system. J Hazard Mater 2010;183(1–3):902–7.
[16] Tao S, Li C, Fan X, Zeng G, Lu P, Zhang X, et al. Activated coke impregnated with cerium chloride used for elemental mercury removal from simulated flue gas. Chem Eng J 2012;210:547–56.
[17] Yang HM, Pan WP. Transformation of mercury speciation through the SCR system in power plants. J Environ Sci 2007;19(2):181–4.
[18] Pudasainee D, Lee SJ, Lee SH, Kim JH, Jang HN, Cho SJ, et al. Effect of selective catalytic reactor on oxidation and enhanced removal of mercury in coal-fired power plants. Fuel 2010;89:804–9.
[19] Cao Y, Gao Z, Zhu J, Wang Q, Huang Y, Chiu C, et al. Impacts of halogen additions on mercury oxidation, in a slipstream selective catalyst reduction (SCR), reactor when burning sub-bituminous coal. Environ Sci Technol 2008;42(1):256–61.
[20] Hong HJ, Ham SW, Kim M, Lee SM, Lee JB. Characteristics of commercial selective catalytic reduction catalyst for the oxidation of gaseous elemental mercury with respect to reaction conditions. Korean J Chem Eng 2010;27(4):1117–22.
[21] Yang S, Guo Y, Yan N, Wu D, He H, Xie J, et al. Remarkable effect of the incorporation of titanium on the catalytic activity and SO_2 poisoning resistance of magnetic Mn–Fe spinel for elemental mercury capture. Appl Catal B: Environ 2011;101(3–4):698–708.
[22] Tan Z, Su S, Qiu J, Kong F, Wang Z, Hao F, et al. Preparation and characterization of Fe_2O_3–SiO_2 composite and its effect on elemental mercury removal. Chem Eng J 2012;195–196:218–25.
[23] Zhang A, Zheng W, Song J, Hu S, Liu Z, Xiang J. Cobalt manganese oxides modified titania catalysts for oxidation of elemental mercury at low flue gas temperature. Chem Eng J 2014;236:29–38.
[24] Lee KJ, Kumar PA, Maqbool MS, Rao KN, Song KH, Ha HP. Ceria added Sb–V_2O_5/TiO_2 catalysts for low temperature NH_3 SCR: physico-chemical properties and catalytic activity. Appl Catal B: Environ 2013;142–143:705–17.
[25] Lee SM, Park KH, Hong SC. MnO_x/CeO_2–TiO_2 mixed oxide catalysts for the selective catalytic reduction of NO with NH_3 at low temperature. Chem Eng J 2012;195–196:323–31.
[26] Shen B, Yao Y, Ma H, Liu T. Ceria modified MnO_x/TiO_2-pillared clays catalysts for the selective catalytic reduction of NO with NH_3 at low temperature. Chin J Catal 2011;32:1803–11.
[27] Pârvulescu VI, Boghosian S, Pârvulescu V, Jung SM, Grange P. Selective catalytic reduction of NO with NH_3 over mesoporous V_2O_5–TiO_2–SiO_2 catalysts. J Catal 2003;217(1):172–85.
[28] Li HL, Li Y, Wu CY, Zhang JY. Oxidation and capture of elemental mercury over SiO_2–TiO_2–V_2O_5 catalysts in simulated low-rank coal combustion flue gas. Chem Eng J 2011;169(1–3):186–93.
[29] Xie JK, Yan NQ, Yang SJ, Qu Z, Chen WM, Zhang WQ, et al. Synthesis and characterization of nano-sized Mn–TiO_2 catalysts and their application to removal of gaseous elemental mercury. Res Chem Intermed 2012;38(9):2511–22.
[30] Xu W, Yu Y, Zhang C, He H. Selective catalytic reduction of NO by NH_3 over a Ce/TiO_2 catalyst. Catal Commun 2008;9(6):1453–7.
[31] Gao X, Jiang Y, Fu Y, Zhong Y, Luo Z, Cen K. Preparation and characterization of CeO_2/TiO_2 catalysts for selective catalytic reduction of NO with NH_3. Catal Commun 2010;11(5):465–9.
[32] Shan W, Liu F, He H, Shi X, Zhang C. An environmentally-benign CeO_2–TiO_2 catalyst for the selective catalytic reduction of NO_x with NH_3 in simulated diesel exhaust. Catal Today 2012;184:160–5.
[33] Li HL, Wu CY, Li Y, Zhang JY. CeO_2–TiO_2 catalysts for catalytic oxidation of elemental mercury in low-rank coal combustion flue gas. Environ Sci Technol 2011;45(17):7394–400.
[34] Shan W, Liu F, He H, Shi X, Zhang C. An environmentally-benign CeO_2–TiO_2 catalyst for the selective catalytic reduction of NO_x with NH_3 in simulated diesel exhaust. Catal Today 2012;184(1):160–5.
[35] Wan Q, Duan L, He KB, Li JH. Removal of gaseous elemental mercury over a CeO_2–WO_3/TiO_2 nanocomposite in simulated coal-fired flue gas. Chem Eng J 2011;170(2–3):512–7.
[36] Campbell CT, Peden CH. Oxygen vacancies and catalysis on ceria surfaces. Science 2005;309(5735):713–4.
[37] Li H, Wu CY, Li Y, Zhang J. Superior activity of MnO_x–CeO_2/TiO_2 catalyst for catalytic oxidation of elemental mercury at low flue gas temperatures. Appl Catal B: Environ 2012;111–112:381–8.
[38] Gao X, Jiang Y, Zhong Y, Luo Z, Cen K. The activity and characterization of CeO_2–TiO_2 catalysts prepared by the sol–gel method for selective catalytic reduction of NO with NH_3. J Hazard Mater 2010;174(1–3):734–9.
[39] Shan W, Liu F, He H, Shi X, Zhang C. A superior Ce–W–Ti mixed oxide catalyst for the selective catalytic reduction of NO*x* with NH_3. Appl Catal B: Environ 2012;115:100–6.
[40] Fang J, Bi X, Si D, Jiang Z, Huang W. Spectroscopic studies of interfacial structures of CeO_2–TiO_2 mixed oxides. Appl Surf Sci 2007;253(22):8952–61.
[41] Wu Z, Jin R, Liu Y, Wang H. Ceria modified MnO_x/TiO_2 as a superior catalyst for NO reduction with NH_3 at low-temperature. Catal Commun 2008;9(13):2217–20.
[42] Yu D, Liu Y, Wu Z. Low-temperature catalytic oxidation of toluene over mesoporous MnO_x–CeO_2/TiO_2 prepared by sol–gel method. Catal Commun 2010;11(8):788–91.
[43] Reddy BM, Khan A, Yamada Y, Kobayashi T, Loridant S, Volta JC. Structural characterization of CeO_2–TiO_2 and V_2O_5/CeO_2–TiO_2 catalysts by Raman and XPS techniques. J Phys Chem B 2003;107(22):5162–7.
[44] He H, Dai H, Au C. Defective structure, oxygen mobility, oxygen storage capacity, and redox properties of RE-based (RE = Ce, Pr) solid solutions. Catal Today 2004;90(3):245–54.
[45] Mao XB, Gao YQ, Gong MC. High performance $Ce_{0.35}Zr_{0.55}Y_{0.1}O_{1.95}$ rare earth oxygen storage material, Chinese. J Inorg Chem 2006;22(8):1521–4.
[46] Lindström R, Maurice V, Groult H, Perrigaud L, Zanna S, Cohen C, et al. Li-intercalation behaviour of vanadium oxide thin film prepared by thermal oxidation of vanadium metal. Electrochim Acta 2006;51(23):5001–11.
[47] He S, Zhou JS, Zhu YQ, Luo ZY, Ni MJ, Cen KF. Mercury oxidation over a vanadia-based selective catalytic reduction catalyst. Energy Fuel 2009;23(1):253–9.
[48] He J, Reddy GK, Thiel SW, Smirniotis PG, Pinto NG. Ceria-modified manganese oxide/titania materials for removal of elemental and oxidized mercury from flue gas. J Phys Chem C 2011;115(49):24300–9.
[49] Li Y, Murphy PD, Wu CY, Powers KW, Bonzongo JCJ. Development of silica/vanadia/titania catalysts for removal of elemental mercury from coal-combustion flue gas. Environ Sci Technol 2008;42(14):5304–9.
[50] Granite EJ, Pennline HW, Hargis RA. Novel sorbents for mercury removal from flue gas. Ind Eng Chem Res 2000;39(4):1020–9.
[51] Jin R, Liu Y, Wu Z, Wang H, Gu T. Low-temperature selective catalytic reduction of NO with NH_3 over MnCe oxides supported on TiO_2 and Al_2O_3: a comparative study. Chemosphere 2010;78(9):1160–6.
[52] Fan X, Li C, Zeng G, Gao Z, Chen L, Zhang W, et al. Removal of gas-phase element mercury by activated carbon fiber impregnated with CeO_2. Energy Fuel 2010;24:4250–4.
[53] Li H, Wu CY, Li Y, Li L, Zhao Y, Zhang J. Role of flue gas components in mercury oxidation over TiO_2 supported MnO_x–CeO_2 mixed-oxide at low temperature. J Hazard Mater 2012;243:117–23.
[54] Li H, Wu CY, Li Y, Li L, Zhao Y, Zhang J. Impact of SO_2 on elemental mercury oxidation over CeO_2–TiO_2 catalyst. Chem Eng J 2013;219:319–26.
[55] Zhou J, Hou W, Qi P, Gao X, Luo Z, Cen K. CeO_2–TiO_2 sorbents for the removal of elemental mercury from syngas. Environ Sci Technol 2013;47(17):10056–62.
[56] Kim MH, Ham SW, Lee JB. Oxidation of gaseous elemental mercury by hydrochloric acid over $CuCl_2$/TiO_2-based catalysts in SCR process. Appl Catal B: Environ 2010;99(1–2):272–8.